HHS Public Access

Author manuscript

Arch Biochem Biophys. Author manuscript; available in PMC 2019 June 15.

Published in final edited form as:

Arch Biochem Biophys. 2018 June 15; 648: 27–35. doi:10.1016/j.abb.2018.04.014.

ROLE OF THE C-TERMINUS MOBILE DOMAIN OF CARDIAC TROPONIN I IN THE REGULATION OF THIN FILAMENT ACTIVATION IN SKINNED PAPILLARY MUSCLE STRIPS

Nazanin Bohlooli Ghashghaee[a], **King-Lun Li**[a], **R. John Solaro**[b], and **Wen-Ji Dong**[a,c]

[a]The Gene and Linda Voiland School of Chemical Engineering and Bioengineering, Washington State University, Pullman, WA 99164, USA

[b]The Department of Physiology and Biophysics, Center for Cardiovascular Research, College of Medicine, University of Illinois at Chicago, Chicago, IL 60612, USA

[c]The Department of Integrative Physiology and Neuroscience, Washington State University, Pullman, WA 99164, USA

Abstract

The C-terminus mobile domain of cTnI (cTnI-MD) is a highly conserved region which stabilizes the actin-cTnI interaction during the diastole. Upon Ca^{2+}-binding to cTnC, cTnI-MD participates in a regulatory switching that involves cTnI to switch from interacting with actin toward interacting with the Ca^{2+}-regulatory domain of cTnC. Despite many studies targeting the cTnI-MD, the role of this region in the length-dependent activation of cardiac contractility is yet to be determined. The present study investigated the functional consequences of losing the entire cTnI-MD in cTnI(1-167) truncation mutant, as it was exchanged for endogenous cTnI in skinned rat papillary muscle fibers. The influence of cTnI-MD truncation on the extent of the N-domain of cTnC hydrophobic cleft opening and the steady-state force as a function of sarcomere length (SL), cross-bridge state, and [Ca^{2+}] was assessed using the simultaneous *in situ* time-resolved FRET and force measurements at short (1.8 μm) and long (2.2 μm) SLs. Our results show the significant role of cTnI-MD in the length dependent thin filament activation and the coupling between thin and thick filament regulations affected by SL. Our results also suggest that cTnI-MD transmits the effects of SL change to the core of troponin complex. [1]

Keywords

Troponin; cardiac troponin I; Förster Resonance Energy Transfer (FRET); Length dependent activation; cross-bridge; mobile domain truncation

Disclosures

No conflicts of interest, financial or otherwise, are declared by the author(s).

1. Introduction

The Frank-Starling law of the heart describes beat-to-beat regulation of ventricular function by adjusting ventricular pressure and stroke volume in response to the extent of ventricular filling [1–3]. An increase in end diastolic volume stretches the muscular walls and therefore increases the length of myocardial sarcomeres thereby increasing muscle force generation and pressure [2]. An increase in sarcomere length (SL) is associated with the enhancement of myofilament Ca^{2+}-sensitivity [4–6] and the contractile force of the left ventricle [2, 4, 6, 7]. This cellular mechanism is commonly referred to as myofilament length dependent activation (LDA) [8]. Despite extensive efforts, the molecular mechanism underlying LDA is still elusive [8–12].

Previous studies suggest a complex dynamic interplay between different components of the myofilament in LDA, including inter-filament lattice spacing [13–15], titin-based passive tension [16–21], the orientation and number of cross-bridges [22–24], as well as the distinctive structural changes in both thin and thick filaments [25, 26]. Moreover, an increase in SL has been associated with the increased probability of strong cross-bridge force generating reactions at a given Ca^{2+} concentration [3, 27–32], which exerts a positive feedback on myocardial contractile regulation [33–38]. This feedback mechanism has been suggested to be a consequence of myosin-induced movement of tropomyosin from a closed- to open-state position on the thin filament [37]. Strong cross-bridges have been found to sensitize the myofilament to Ca^{2+} and stabilize the interaction between the switch region of cardiac troponin I (cTnI) and the N-domain of cardiac troponin C (N-cTnC) [39]. However, it is still unknown how myofilament Ca^{2+}-sensitivity is regulated by SL, so there is a strong need to solve this fascinating molecular physiology mystery.

To understand the role of SL on Ca^{2+} mediated thin filament regulation, as well as the role of different cross-bridge states in LDA, our group developed an *in situ* optical-mechanical approach to study thin filament regulation at the molecular level [10, 39]. Ca^{2+}-binding to N-cTnC, which triggers systole, is accompanied by a series of conformational changes in the thin filament proteins [40–42]. It starts with partially exposing a previously buried hydrophobic cleft in N-cTnC [10, 43–45], followed by the interaction between the switch region of cTnI and the hydrophobic cleft of N-cTnC [46–49]. Consequently, interactions of the inhibitory and switch regions of cTnI with actin is no longer favored and an interaction with N-cTnC [44, 45, 47–52] occurs and further stabilizes the Ca^{2+}-induced N-cTnC opening [44, 45, 51, 52]. These Ca^{2+}-induced structural changes are believed to be sensitive to changes in SL and cross-bridge states and are expected to be involved in LDA [10, 53].

Considering SL-induced increase in Ca^{2+}-sensitivity is a key characteristic of LDA and cTnC is the myofilament Ca^{2+} sensor, simultaneous monitoring of Ca^{2+}-induced opening of N-cTnC and mechanical force development of cardiac muscle fibers at various SLs and cross-bridge states can help to acquire information on how conformational changes in N-cTnC responds to the molecular mechanism underlying the LDA. In our previous studies, *in situ* time-resolved Förster resonance energy transfer (FRET) measurements in chemically skinned muscle fibers were performed to monitor the opening of N-cTnC [10, 39], which is the triggering step of the thin filament regulation. The results revealed that Ca^{2+}-induced

opening of the N-cTnC is SL dependent, and strongly bound cross-bridges play an important role in the modulation of myofilament activation by SL [10].

Among thin filament proteins, cTnI, a key component of Ca^{2+}-activation [50, 52–54], is shown to be involved in LDA [53, 55–57]. The C-terminus of cTnI which plays a critical role in the regulatory function of cTnI, is composed of three functional regions: the inhibitory region, the switch region, and the mobile domain (cTnI-MD). The cTnI-MD (residues 168-210) plays an important role in the regulatory switching of cTnI interacting with actin and N-cTnC. The cTnI-MD is shown to stabilize the interaction between cTnI and actin at the relaxed state of thin filament [58–60]. NMR studies [61–63] and H/D-exchange-mass-spectrometry [64, 65] have suggested a slow dynamics for cTnI-MD at relaxed state which denotes its rigid actin-binding conformation, and a highly dynamic behavior at activated state [52, 59, 62]. These studies suggest a vital role of cTnI-MD in the kinetics of thin filament regulation through “fly-casting mechanism” due to an intrinsically disordered nature of this region in solution [66]. Our recent study [56] using skinned rat papillary muscle fibers containing truncated cTnI, cTnI(1-167), revealed that the cTnI-MD truncation diminished the SL-induced increase in Ca^{2+}-sensitivity of contraction, but not the SL-dependent increase in maximal tension, showing an uncoupling between the thin and thick filament contributions to LDA. While important information has been uncovered regarding the role of the cTnI-MD in cardiac contractility and LDA, an ongoing question is how cTnI-MD affects the structural transitions within thin filament and force production under different cross-bridge states as SL varies.

In this study, we engineered a cTnI construct in which the entire mobile domain is truncated, cTnI(1-167). The cTnI(1-167) was reconstituted along with rat cTnT and rat AEDANS-DDPM-modified cTnC(T13C/N51C), and subsequently exchanged into skinned rat papillary muscle fibers. *In situ* time-resolved FRET technique using time-correlated single-photon counting technology was implemented to investigate the functional significance of cTnI-MD in Ca^{2+}-, cross-bridge-, and SL-induced opening of the hydrophobic cleft of the N-cTnC. In this study, the tested cross-bridge states included: the cycling cross-bridges (ATP state); Mg^{2+}ADP-induced non-cycling strong binding cross-bridges (ADP state); and Vanadate-induced non-cycling weak-binding cross-bridges (Vi state). Our results indicate that the entire cTnI-MD truncation blunts the SL-induced opening of N-cTnC under both ATP and ADP treatments by enhancing the opening of N-cTnC at short SL to match that of the long SL and this truncation uncouples the thin filament and thick filament-based regulations of LDA.

2. Materials and methods

2.1. Animal handling protocols

The handling of all the experimental animals followed the Institutional Animal Care and Use Committee at Washington State University and the Office of Laboratory Animal Welfare, National Institute of Health, Bethesda, MD. Our muscle preparations study followed the established guidelines of and was approved by the Washington State University Institutional Animal Care and Use Committee. Rats were deeply anesthetized by isoflurane inhalation

(3% volume in 95% O_2-5% CO_2 flowing at 2 l/min), following which hearts were immediately excised and placed into ice-cold dissecting solution.

2.2. Preparation of proteins

The recombinant double-cysteine mutant cTnC(T13C/N51C), as well as the C-terminus truncation of cTnI, cTnI(1-167), from a rat cDNA clone were sub-cloned into a pET-3d vector. The mutant clones were then transformed into BL21(DE3) cells and expressed under isopropyl β-D-1-thiogalactopyranoside induction. The expressed proteins were purified as previously described [39, 45, 46, 49]. The mutant cTnC was then fluorescently labeled with the FRET donor AEDANS using thiol-reactive 5-(iodoacetamidoethyl) aminonaphthelene-1-sulfonic acid as previously described [39]. The DEAE column was used to separate the unlabeled, singly and doubly labeled cTnC(T13C/N51C). The concentrated singly labeled fraction of cTnC(T13C/N51C)$_{AEDANS}$ (donor-only sample), was collected and divided into two parts. One part was saved as reference sample (donor-only sample), and the other part was subsequently labeled with the excess amount of FRET acceptor DDPM at the other cysteine to achieve the doubly labeled cTnC(T13C/N51C)$_{AEDANS\text{-}DDPM}$ (donor-acceptor sample). The labeling ratio of the donor-only sample was verified to be >95% using UV-vis spectroscopy and the $\varepsilon_{325\ nm}$ of AEDANS, which is 6000 cm^{-1} M^{-1}.

2.3. Preparation of pCa solutions

Solution concentrations were formulated based on calculations of the program by Fabiato [67], with all concentrations reported in mM unless otherwise noted. The 20 mM ethylene glycol-bis(β-aminoethyl ether)-N,N,N′,N′-tetraacetic acid (EGTA) relaxing solution contained 20 EGTA, 50 N,N-Bis(2-hydroxyethyl)-2-aminoethanesulfonic acid (BES), 30.83 K-propionate, 10 sodium azide (NaN_3), 6.29 $MgCl_2$, and 6.09 Na_2ATP. The activating solution (pCa 4.3) contained 50 BES, 5 NaN_3, 10 EGTA, 10.11 $CaCl_2$, 6.61 $MgCl_2$, 5.95 Na_2ATP, and 51 K-propionate. Our relaxing solution (pCa 9) was composed of 50 BES, 5 NaN_3, 10 EGTA, 0.024 $CaCl_2$, 6.87 $MgCl_2$, 5.83 Na_2ATP, and 71.14 K-propionate. To promote the ADP-mediated non-cycling, strong-binding cross-bridge interactions, ATP in the activating and relaxing solutions was replaced with 5 mM Mg^{2+}ADP. To inhibit cross-bridge interactions, 1 mM sodium Vi was added to the above pCa solutions. The ionic strength of all pCa solutions was 180 mM. Protease inhibitors including 5 μM bestatin, 2 μM E-64, 10 μM leupeptin, and 1 μM pepstatin were also added to these solutions [68].

2.4. Preparation of detergent-skinned cardiac muscle fibers

Left ventricular papillary muscle bundles were dissected from 5 hearts of adult (4-6 months in age) Sprague Dawley rats and pared down to thin fibers (~150-200 μm in diameter and 2.0 mm in length) using previously established protocols [10, 39, 69]. After the hearts were excised, they were placed into ice-cold 20mM EGTA relaxing solution in the presence of 1.0 mM dithiothreitol (DTT), and 20 mM 2, 3-butanedione monoxime (BDM). Fresh protease inhibitors including 4 mM benzamidine-HCl, 5 mM bestatin, 2 mM E-64, 10 mM leupeptin, 1 mM pepstatin and 200 mM phenylmethyl-sulfonyl fluoride were added to the solution. Muscle fibers were dissected and skinned overnight at 4 °C using 1% triton X-100 in 20 mM EGTA relaxing solution.

2.5. Incorporation of cTnI(1-167) and fluorescently labeled cTnC constructs into detergent skinned myocardial fibers

In the previous study by our group [10], the extraction/replacement protocol using CDTA was used to incorporate fluorescently labeled cTnC into cardiac muscle fibers. However, the CDTA extraction procedure causes muscle fibers to shrink substantially. Also, CDTA extraction method may leave some parts of myofilament lacking cTnC or myosin regulatory light chain. In this study, to address such issues caused by CDTA extraction, we implement a whole troponin exchange protocol, which does not require CDTA extraction.

Troponin complex containing cTnC(T13C/N51C)$_{AEDANS\text{-}DDPM}$, cTnI(1-167), and the wild-type cTnT was reconstituted at a molar ratio of 1:1:1 cTnC:cTnI:cTnT using a protocol published previously [10, 53]. The endogenous troponin in the detergent skinned muscle fibers were exchanged by overnight incubation in exchange solution containing 25 μM of reconstituted cTn complex followed by another overnight incubation of fibers in exchange solution containing 10 μM of only cTnC. The exchange solution contained (in mM): 50 BES, 30.83 K-propionate, 10 NaN_3, 20 EGTA, 6.29 $MgCl_2$, 6.09 Na_2ATP, 10 BDM,1 DTT, 0.005 bestatin, 0.002 E-64, 0.01 leupeptin, and 0.001 pepstatin. For the donor-only samples the same exchange protocol was followed, but cTnC(T13C/N51C)$_{AEDANS\text{-}DDPM}$ was replaced with cTnC(T13C/N51C)$_{AEDANS}$. The same exchange procedure was followed using wild-type cTnI that served as our control fibers.

One potential issue with whole troponin exchange is that the capability to replace endogenous proteins by each troponin subunit may be different, which may lead to non-uniform exchange ratio of cTnC(13C-51C)$_{AEDANS\text{-}DDPM}$ to cTnI. Although the whole troponin exchange protocol is not perfect, the mechanic behavior of the reconstituted fibers is much better than the ones exposed to CDTA.

2.6. Western blotting analysis of reconstitution levels of modified cTnI in cardiac muscle fibers

To evaluate the efficiency of the protein exchange using our protocol, the reconstituted muscle fibers containing cTnI(1-167) was incubated in 10 μL of a protein extraction buffer per 1 muscle fiber on ice for 1 h. The control sample was created using the skinned muscle fibers that had not undergone exchange. The protein extraction buffer contained 2.5% SDS, 10% glycerol, 50 mM Tris-base (pH 6.8 at 4 °C), 1 mM DTT, 1 mM phenylmethylsulfonyl fluoride, 4 mM benzamidine-HCl, 5 μM bestatin, 2 μM E-64, 10 μM leupeptin and 1 μM pepstatin. The procedure was followed by a 20 minute sonication of samples in a water bath at 4 °C and centrifugation at 10k rpm. Equal amounts of supernatants fractions were loaded into 4-20% SDS-PAGE gels for Western blotting analysis following the protocol established previously [39]. The incorporation of cTnI(1-167) was assessed using a primary antibody against cTnI (Abcam #19615) followed by horseradish peroxidase conjugated anti-mouse antibody (GE healthcare NXA931). The exchange ratio of the truncated cTnI-MD with the endogenous cTnI was calculated as the ratio of the density of the band for truncated cTnI-MD to the density of the band for the wild-type cTnI in the same lane.

2.7. Simultaneous measurements of isometric force and time-resolved FRET in detergent-skinned cardiac muscle fibers

To conduct synchronized measurements of force and time-resolved FRET of N-cTnC opening, the measurements protocol described previously was followed [10, 39]. The protocol scheme for simultaneous fluorescence lifetime and isometric force measurements at different cross-bridge states is shown at Fig. 1. The simultaneous monitoring of biomechanical and optical measurements was done using Güth MRS OPT modified with a TBX picosecond photon detection module (HORIBA Jobin Yvon) which allows using the time-correlated single-photon counting technology for fluorophore lifetime determination. Briefly, to perform the measurements, the skinned muscle fiber was mounted onto the force transducer (SI Heidelberg KG7A) and a stationary tweezer. The force transducer capable of measuring 5 mN with a resonance frequency of 500 Hz was used to perform the isometric force measurements. A quartz perfusion cuvette with a diameter of 1 mm was slipped over the preparation and pCa solution was continuously perfused through the mounted fiber during experimentation. The SL of the muscle fiber was then adjusted to either 1.8 or 2.2 μm using He-Ne laser diffraction measurements. The bipolar temperature controller (Cell Micro-Controls TC2BIP) coupled with a cooling/heating module (Cell MicroControls CH) was used to maintain the experimental temperature of the pCa solutions at 20 ± 0.2 °C. Excitation light at 340 nm was projected onto the muscle fiber through the cuvette from a NanoLED (HORIBA Jobin Yvon N-340) with a < 1.2 ns pulse width and a 460 nm cutoff filter. The total fluorescence emission from the central area of the muscle fiber was isolated for measurement. Fluorescence intensity decays of muscle fibers containing either donor-only or donor-acceptor modified cTnC(T13C/N51C) were processed and recorded by a FluoroHub-B (HORIBA Jobin Yvon). With this instrument setup, a total of 10,000 photon counts at peak channel for each decay collection was achieved in 1–1.5 min. Time-resolved measurements were conducted when force reached steady state to exclude the uncontrolled factors that can affect protein conformation during the rising phase of force development (Fig.1) For more information regarding the experimental apparatus please refer to our previous publication [10, 53].

To eliminate experimental uncertainty from variations in handling between fiber preparations, same muscle fiber was used to perform isometric force and time-resolved fluorescence measurements at both 1.8 and 2.2 μm SLs, according to the following measurement protocol. Half of our measurements were started at 1.8 μm SL, whereas the other half was started at 2.2 μm SL. The SL was adjusted to either 1.8 or 2.2 μm SL using laser diffraction and subjected to an initial cycle of activation and relaxation. Isometric force and a fluorescence lifetime decay were then synchronously and digitally recorded as the fiber was subjected to pCa 4.3 solution at the chosen SL. This followed by the addition of highly relaxing solution, containing 20 mM EGTA, to completely relax the fiber. The SL of the fiber was then adjusted to the opposite SL of the one that was initially chosen; for example, if the measurement had started with 2.2 μm SL, then the fiber was adjusted to a SL of 1.8 μm. Measurements were performed using the same procedure as before. The order with which SLs were tested was later found not to affect the outcome of experiments.

The time-resolved FRET measurements of N-cTnC opening were performed in the presence of cycling cross-bridges (5 mM Mg^{2+}ATP); Mg^{2+}ADP -induced non-cycling, strong-binding cross-bridges (5 mM MgADP + 0 mM ATP); and Vi-induced non-cycling, weak-binding cross-bridges (1 mM Vi + 5 mM Mg^{2+}ATP). There are some important experimental design considerations for using Vi to inhibit strong cross-bridge binding [70–73], and we have previously demonstrated that using low concentration of Vi works reliably under our experimental conditions [39, 53]. In our case, regardless of test condition and following the FRET measurement protocol, we confirmed that the maximal force could be recovered on average to 85.0 ± 2.1%. Moreover, no significant change in passive tension at pCa 9 was observed following the time-resolved FRET measurement protocol conducted under Vi treatment.

2.8. Determination of inter-probe distance distribution from measured fluorescence intensity decays

The distribution of inter-probe distance of AEDANS-DDPM associated with a specific test condition using time-correlated single-photon counting technique was determined as follows. The excited-state decays observed for donor-only AEDANS samples were fitted to a double-exponential function [74]:

$$I_D(t) = \sum_{i=1}^{n} \alpha_i e^{-t\tau_i^{-1}} \quad (1)$$

where the α_i represents the fractional amplitude associated with each correlation time τ_i that contributes to the overall excited-state decay process. In the presence of the non-fluorescent acceptor DDPM, the AEDANS excited-state decays observed for donor–acceptor samples were fit to the following equation using DecayFit 1.4 (Fluorescence Decay Analysis Software, FluorTools):

$$I_{DA}(t) = \frac{\int_0^{\infty} P(r)\left(\sum_{i=1}^{n} \alpha_{D_i} e^{-\frac{t}{\tau_{D_i}}\left(1+\left(\frac{R_0}{r}\right)^6\right)}\right)dr}{\int_0^{\infty} P(r)dr} \quad (2)$$

where r is the distance between the donor and acceptor fluorophores; α_{D_i} and τ_{D_i} are the fractional amplitude and correlation time parameters, respectively, determined for AEDANS in the absence of DDPM. R_o is the Förster critical distance at which energy transfer is 50% efficient, and was calculated from the spectral properties of AEDANS and DDPM:

$$R_0 = (8.79 \times 10^{-5}) n^{-4} Q \kappa^2 J \quad (3)$$

where n is the refractive index of the solution which was assumed to be 1.4, Q is the donor quantum yield, κ^2 is the orientation factor, and J is the spectral overlap integral that is given by:

$$J = \frac{\int F_D(\lambda)\varepsilon_A(\lambda)\lambda^4 d\lambda}{\int F_D(\lambda)d\lambda} \quad (4)$$

where $F_D(\lambda)$ is the fluorescence intensity of the donor at wavelength λ and $\varepsilon_A(\lambda)$ is the molar absorptivity of the acceptor at λ. J was calculated by numerical integration. The Cys-13 and Cys-51 of cTnC are both located in surface-exposed loops so the dynamic averaging and the associated value of $\frac{2}{3}$ for κ^2 were assumed. The R_0, which determines sensitivity of FRET between a specific donor and acceptor pair to distance changes, is about 28 Å for the AEDANS-DDPM.

P(r) in Eq. 2 is the probability distribution of inter-probe distances, and in this study, we assume it to be a single Gaussian as follows:

$$P(r) = \frac{1}{Z\sigma\sqrt{2\pi}} e^{-\frac{1}{2}\left(\frac{r-\bar{r}}{\sigma}\right)^2} \quad (5)$$

where r is the mean distance and σ is the standard deviation of the distribution. $P(r)$ is normalized by area, and Z is the normalization factor. The integration limits in Eq. 5 are calculated over a range of distances from $r_{\min}$ to $r_{\max}$ with the lower limit being about 5 Å.

Due to the locations of Cys-13 and Cys-51 within the quaternary structure of N-cTnC, “r” represents the ensemble-averaged extent of N-cTnC hydrophobic cleft exposure [39]. Thus, when a greater population of N-cTnC ensemble transitions from the closed to the open conformation of N-cTnC [44, 75], r increases. The spread of the distance distribution between Cys-13–Cys-51 of N-cTnC transitioning between the conformational sub-states is described by a half-width at half-maximum (HWHM). The equilibrium between the closed and open conformations with significantly different extents of ensemble-averaged opening results in a broadened HWHM.

To fit the AEDANS excited-state decays observed for donor–acceptor samples, using DecayFit 1.4 (Fluorescence Decay Analysis Software, FluorTools), the predefined FRET decay model was used. The model implements a Gaussian distance distribution between the donor and acceptor with the distribution center (r-mean) and Full Width at Half Maximum as fitting parameters. The critical distance, R_0, as well as two lifetimes for donor in absence of acceptor (τ_{D_1} and τ_{D_2}), each with a pre-exponential factor (α_{D_1} and α_{D_2}) must be supplied as input and is not meant to be a fitting parameter. Dynamic averaging and single Gaussian distribution was assumed to fit the FRET data, so the donor-acceptor distance is the mean of the Gaussian distribution (r-mean).

3. Statistical Data Analysis

All values are means ± SE. The three-way ANOVA followed by Tukey post-test was used to examine the influence of SL, truncation, cross-bridge state, and the interaction effect between these three independent variables on the contractile and conformational parameters at each pCa. All statistical analysis was done using GraphPad Prism 7.01. Statistical significance is reported at $P < 0.05$.

4. Results

4.1. Western blot analysis of the reconstituted cardiac muscle fibers

To estimate the relative incorporation of cTnI(1-167) into the samples, equal quantities of digested muscle fiber samples were separated on SDS-PAGE gels for Western blotting analysis (see Methods). The differences in migration speed between the cTnI(1-167) and the endogenous cTnI showed 60% ± 4 relative incorporation of cTnI(1-167) in skinned cardiac muscle fibers.

4.2. Effects of sarcomere length and cTnI-MD truncation on the conformational transitions of N-domain of cTnC

The *in situ* conformational changes of N-cTnC was quantitatively characterized using time-resolved FRET measurements performed on myocardial fibers reconstituted with cTnC(T13C/N51C)$_{AEDANS}$ as a donor-only sample or cTnC(T13C/N51C)$_{AEDANS\text{-}DDPM}$ as a donor-acceptor sample. The AEDANS intensity decay observed under each test condition was analyzed in terms of FRET distance between N-cTnC(Cys-13) and N-cTnC(Cys-51). The mean distances (r) and HWHM recovered from analysis of intensity decay measurements for fibers containing cTnI(WT) and cTnI(1-167) are summarized in Table 1. As described below, changes in r and HWHM were used to evaluate the effects of cTnI-MD truncation, cross-bridge state, and SL on the conformational behavior of N-cTnC at both relaxed and activated states. We will first discuss the results at each section at the relaxed state (pCa 9), followed by the results at activated state (pCa 4.3).

At relaxed state—We will first focus on the effects of SL on the structural transitions of the N-cTnC for each of the cTnI(WT) and cTnI(1-167) reconstituted muscle fibers at different cross-bridge states and then explain how cTnI(1-167) affects these transitions at the relaxed state (pCa 9). Our results from three-way ANOVA show that in absence of Ca^{2+}, increase in SL results in a significant increase in the opening of N-cTnC hydrophobic cleft for cTnI(WT) fibers just under ADP treatment (2.03 ± 0.56 Å increase in r; $P < 0.001$; Fig. 3; Table 1). Among all three cross-bridge states, cTnI(WT) fibers show a greater HWHM at longer SL just under ATP treatment, which indicates that the shift in equilibrium from closed to open conformation is accompanied by more underlying conformational sub-states at ATP state. Increase in SL did not affect the N-cTnC cleft opening and HWHM for cTnI(1-167) fibers under any of the cross-bridge states at relaxed state (Table 1).

At short SL, the cTnI(1-167) resulted in a significant 1.43 ± 0.61 Å increase in r under ADP treatment compared to cTnI(WT) at relaxed state (Fig 3). The cTnI(1-167) did not significantly alter the HWHM compared to cTnI(WT) fibers at short SL.

At long SL, the cTnI(1-167) did not affect the extent of N-cTnC opening in any of three cross-bridge states (Fig. 3). However, the cTnI(1-167) significantly reduced HWHM at long SL, compared to cTnI(WT), which indicates an equilibrium between fewer conformational sub-states after truncating the entire cTnI-MD (Table 1).

At activated state—At saturating Ca^{2+} level (pCa 4.3), increase in SL for fibers containing cTnI(WT) resulted in a significant 2.60 ± 0.77 Å and 3.56 ± 0.62 Å increase in r in the presence of normal cycling and strong-binding cross-bridges, respectively (Fig. 3 and Table 1). At pCa 4.3, increase in SL resulted in a greater HWHM for cTnI(WT) just under normal cross-bridge cycling condition, which implies more conformational sub-states with the shift in equilibrium from closed to open conformation (Table 1). In contrast to cTnI(WT) fibers, increase in SL did not affect either of r or HWHM for cTnI(1-167) fibers under any of the cross-bridge states (Fig. 3 and Table 1).

At short SL, the cTnI(1-167) fibers showed a greater r value compared to cTnI(WT) fibers under both normal cycling and strong binding cross-bridge states (Fig. 3). No significant difference in HWHM was observed with the cTnI(1-167) truncation under any of the cross-bridge states at short SL (Table 1).

At long SL, the cTnI(1-167) did not influence the ensemble-averaged opening of the N-cTnC compared to cTnI(WT) fibers at any of the cross-bridge states (Fig. 3). However, it showed a significantly lower HWHM under normal cross-bridge cycling condition, which denotes that N-cTnC is more stabilized at open state after truncating cTnI-MD (Table 1).

4.3. Effects of cross-bridge states on the conformational transitions of N-domain of cTnC for fibers containing cTnI(WT) or cTnI(1-167)

At relaxed state—At short SL, Fig. 3 shows that in presence of ATP at relaxed state, the N-cTnC ensemble exhibited low r values of 12.30 ± 0.09 and 12.21 ± 0.11 Å for cTnI(WT) and cTnI(1-167) fibers, respectively. Subsequent treatment with Vi to block strong cross-bridge attachment, and treatment with ADP to produce strong-binding non-cycling cross-bridges did not significantly alter r for fibers containing either of cTnI(WT) or cTnI(1-167) (Fig. 3).

At long SL, our results show that in presence of ATP at relaxed state, the N-cTnC ensemble still exhibited low r values of 12.50 ± 0.21 and 12.36 ± 0.06 Å for cTnI(WT) and cTnI(1-167) fibers, respectively. Subsequent treatment with Vi to block strong cross-bridge attachment at long SL did not significantly change the r value for cTnI(WT) nor for cTnI(1-167) fibers. However, treatment with ADP to produce strong-binding cross-bridges resulted in a significant increase in r to the value of 13.81 ± 0.08 Å for cTnI(WT) and caused no significant change for cTnI(1-167) fibers compared to that of ATP state (Fig 3). At long SL, treatment with Vi and ADP both resulted in a significant decrease in HWHM just for cTnI(WT) fibers (Table 1).

At activated state—At short SL, Fig. 3 shows that the ATP treatment at activated state results in greater r values of 21.12 ± 0.74 and 24.37 ± 0.42 Å for cTnI(WT) and cTnI(1-167) fibers, respectively, showing a greater N-cTnC opening by Ca^{2+}. Treatment with Vi

significantly reduced r compared to both ATP and ADP states for both cTnI(WT) and cTnI(1-167) at short SL (Fig. 3). However, ADP treatment did not affect N-cTnC opening compared to normal cross-bridge cycling state for cTnI(WT) nor for cTnI(1-167).

At long SL, similar to short SL, Vi treatment significantly reduced r compared to both ATP and ADP states for both cTnI(WT) and cTnI(1-167) at activated state (Fig. 3). Treatment with ADP did not affect N-cTnC opening compared to ATP state for cTnI(WT) nor for cTnI(1-167). Treatment with both Vi and ADP resulted in a significant decrease in HWHM for cTnI(WT) fibers at long SL (Table 1).

4.4. Effects of cTnI-MD truncation on the steady state isometric force production at different cross-bridge states

Consistent with our previous studies [10, 53], increase in SL at both relaxed and activated states of thin filament results in significant increases in maximal tension in all three cross-bridge states (ATP, Vi, and ADP states) for fibers containing either of cTnI(WT) or cTnI(1-167) (Fig. 4). Force values for fibers containing cTnI(WT) and cTnI(1-167) are summarized in Table 1.

At relaxed state—At short SL and at pCa 9, the cTnI(1-167) did not significantly affect the steady state isometric tension under either of ATP and Vi treatments (Fig. 4). However, the cTnI(1-167) resulted in a significant 11.32 ± 1.63 mN mm^{-2} increase in steady state tension under ADP treatment.

At long SL, the cTnI(1-167) resulted in significant 7.26 ± 2.21 and 5.57 ± 0.80 mN mm^{-2} increases in the isometric tension under ATP and Vi treatments, respectively (Fig. 4). However, no significant change in maximal tension was observed for cTnI(1-167) fibers when treated with ADP compared to cTnI(WT) (Fig. 4).

At activated state—At short SL, the cTnI(1-167) resulted in significant 13.19 ± 2.18 and 10.73 ± 2.50 mN mm^{-2} increases in the maximal isometric tension under ATP and ADP treatments, respectively. Under Vi treatment, this truncation did not affect the maximal tension compared to cTnI(WT) fibers at the same condition (Table 1).

At long SL, the cTnI(1-167) resulted in a significant 13.05 ± 2.09 mN mm^{-2} increase in maximal tension under ATP treatment, compared to cTnI(WT) fibers (Fig. 4). The cTnI(1-167) did not significantly affect the maximal tension under Vi and ADP treatments at long SL and at the activated state of thin filament (Table 1).

5. Discussion

To clarify the molecular mechanisms underlying the role of the cTnI-MD in the modulation of Ca^{2+}-activated troponin regulation by SL, in this study, we investigated how truncating the entire cTnI-MD responds to the effects of the Ca^{2+}, cross-bridges and SL within chemically skinned papillary muscle fibers. Our results suggest that the MD, downstream from the switch region, is critical to the regulatory role of cTnI in modulating myocardial

length dependent activation (LDA) as it balances the interplay between thin and thick filament components of LDA.

The result of our SL-dependent structure-function study for myocardial fibers containing cTnI(WT), is consistent with our previous study noting that in the relaxed state of thin filament, the SL-induced opening of N-cTnC occurs under strong binding cross-bridge treatment [10]. It is worth noting that the FRET distances observed in the current study are shorter than the ones observed in our previous study [10]. The differences are likely caused by different reconstitution protocols that were used for incorporation of the mutant $cTnC(13C\text{-}51C)_{AEDANS\text{-}DDPM}$ into the skinned myocardial fibers. As mentioned in the method section, in the previous study by our group, the CDTA extraction procedure was used [10], which caused the muscle fibers to shrink more than normal skinned fibers. To circumvent the issue, the current study uses whole troponin exchange protocol. The reconstituted fibers in current study are much like normal skinned fibers. In both studies, calcium-induced relative changes in ensemble FRET distances in cTnC are used as a parameter for structural/functional evaluation of troponin regulation. Despite the shorter FRET distances observed in this study, both studies show a similar trend for calcium-induced hydrophobic cleft opening of N-cTnC for fibers containing cTnI(WT). Consistent with our previous study [10], increase in SL together with the feedback effects from strongly bound cross-bridges cause more opening of N-cTnC at the relaxed state for fibers containing cTnI(WT). This observation is believed to be associated with the strong binding myosins promoting the release of the switch region of cTnI from actin and subsequent interaction with N-cTnC. However, cTnI-MD truncation blunts this SL effect under ADP treatment by enhancing the ensemble-averaged N-cTnC opening at short SL to the level of long SL. Our results show that the SL-induced increase in maximal tension is preserved in fibers containing cTnI(1-167) at relaxed state under ADP treatment. This implies that the thick filament-based regulations of LDA reflected by a greater force produced at longer SL is preserved with cTnI-MD truncation but the thin filament-based regulations of LDA reflected by the enhanced N-cTnC opening is abolished. Therefore, our results suggest that truncation of cTnI(1-167) perturbs thin filament-based regulatory mechanisms of LDA and the interplay between thin and thick filament-based regulation mechanisms of LDA, which is consistent with our previous study [56]. A recent study by Zhang et al. also supports our finding that the SL-induced increase in maximal force and N-cTnC opening are not necessarily coupled. They found that the SL-induced enhancement of Ca^{2+} sensitivity is mediated through a direct effect on the structure of troponin in the thin filament and the increase in maximal force is mediated through structural changes of myosin in thick filament [25].

Our finding that the deletion of cTnI-MD induces an increase in N-cTnC opening at short SL under ADP treatment at relaxed state indicates a potential increase in the availability of the cTnI-switch region for N-cTnC at short SL that could result in a greater N-cTnC opening in absence of Ca^{2+}. The cTnI(1-167) lacks the second actin-binding region of the C-terminus of cTnI (residues 170-181) which may lead to a weaker cTnI-actin binding and a more flexible tropomyosin. This may promote the release of the switch region of cTnI from actin under ADP treatment at relaxed state that results in a greater N-cTnC opening at short SL and potentially activates the thin filament. However, at relaxed state, our observation that the

increase in SL under ADP treatment does not further enhance the N-cTnC opening, may imply that the cTnI-MD plays a critical role in sensing and/or transmitting the effects of the change in SL to the regulatory domain of cTnC. It should be noted that our results do not exclude the possibility that the combined effects of the cTnI-MD truncation and strongly bound cross-bridges may saturate the opening of the N-cTnC at the relaxed state of thin filament at short SL. Therefore, further increasing SL would not further enhance these effects. Additional structure-function studies are needed in future to illustrate the detailed regulatory role of different regions of MD in LDA.

At saturating Ca^{2+} concentrations, fibers containing cTnI(WT) showed SL-induced opening of N-cTnC under both ATP and ADP treatments. However, the cTnI(1-167) diminished this SL effect by promoting opening of N-cTnC at short SL to the same extent as long SL (Fig. 3). This observation may be due to the N-cTnC reaching the maximal ensemble-averaged opening at short SL. We speculate that this increase in the N-cTnC opening at short SL could result if i) the cTnI-MD truncation affects the structure and/or orientation of thin filament such that it increases the probability of N-cTnC to interact with the switch region of cTnI and to stabilize this interaction; ii) the cTnI(1-167) truncation causes re-positioning of the tropomyosin on the actin filament such that it increases the probability of strong cross-bridge binding at short SL, which can work in synergy with the positive feedback regulation to shift the conformational equilibrium of N-cTnC more toward the open state. Both scenarios are supported by the observation of the significant decrease in HWHM for fibers containing cTnI(1-167) compared to cTnI(WT) under both ATP and ADP treatments, which shows a more stabilized open conformation of the N-cTnC for cTnI(1-167) fibers. In our study, we rule out the possibility of residual endogenous cTnI masking the effects of the partially exchanged cTnI-MD, since the 60% exchange ratio resulted in a significant increase in the opening of N-cTnC at short SL.

Another finding of this study is that the observed effect of cTnI-MD truncation on the SL-induced opening of N-cTnC is uncoupled from the SL-induced enhancement of maximal force (Fig. 4). Our mechanical measurements showed that the SL-induced increase in maximal force is retained for fibers containing cTnI(WT) or cTnI-MD truncation at both relaxing and activating Ca^{2+} concentrations and under all three cross-bridge states (Fig. 4). The uncoupling between SL effects on force and the extent of N-cTnC opening that was observed for fibers containing cTnI(1-167) implies that the truncation of cTnI-MD likely disrupts the modulation of the thin filament regulation by SL. Interestingly, our data for cTnI(1-167) fibers show that under normal cross-bridge cycling, truncating the cTnI-MD at saturating Ca^{2+} level and at long SL mimics the strong binding cross-bridge (ADP) state in terms of tension development. Increase in maximal tension under normal cross-bridge cycling for cTnI(1-167) may be a result of the repositioning of tropomyosin on thin filament in a way that it resembles its conformation under strong binding cross-bridge state. Our result for cTnI(1-167) is consistent with our previous study which was performed under normal cross-bridge cycling state and showed an uncoupling between SL-induced increase in tension development and Ca^{2+}-sensitivity and cooperativity of contraction [56]. Our results suggest that the effect of cTnI-MD truncation on tension development is more pronounced at short SL at both relaxed and activated states because the increase in SL partly compensates the increased maximal force caused by cTnI-MD truncation (Fig. 4).

Furthermore, at long SL and under Vi treatment, the cTnI(1-167) showed an increase in the amount of force development in the relaxed state compared to cTnI(WT) fibers that highlights the critical role of cTnI-MD in mediating the equilibrium position of tropomyosin between the blocked-, closed-, and open-states on actin filament which can modulate the level of thin filament activation and force development. This mediating role of cTnI-MD is expected at relaxed state by promoting the blocked-state position of tropomyosin. However, the effects of cTnI-MD truncation on the amount of force development at activated state under ATP and ADP treatments may suggest the potential role of the cTnI-MD sampling arm in modulating the equilibrium position of tropomyosin on actin filament at activated state despite dissociation from actin filament.

In summary, our biophysical data presented here implicates the functional significance of the cTnI-MD in length dependent thin filament activation and coupling between thin and thick filament-based regulations of LDA. Our results show that truncating the entire mobile domain disrupts the Length-dependent thin filament regulation which involves greater ensemble-averaged N-cTnC opening at longer SL while the length-dependent increase in maximal tension is preserved. Our observations suggest that the cTnI-MD truncation increases the availability of the switch region of cTnI for the N-cTnC which results in an increase in the population of cTnC with the hydrophobic cleft at open state. In this study, we also show that the effect of cTnI-MD truncation at the level of thin filament activation is more pronounced at short SL, evident by the greater extent of ensemble-averaged N-cTnC opening in cTnI(1-167) fibers compared to cTnI(WT) fibers at short SL. Altogether, our mechanical force measurements and FRET measurements revealed the significance of cTnI-MD in modulating the level of thin filament activation and the potential role of this region in blocked- to closed- to open-state transition(s) of tropomyosin on actin filament at both relaxed and activated states. Additional works in future are needed to characterize the thin filament backbone dynamics after cTnI-MD truncation. Future studies such as 3D reconstructions from electron micrographs for fibers containing cTnI-MD truncations may provide us a better understanding of the role of MD in thin filament-based regulations of LDA.

Acknowledgments

This work is supported by National Institutes of Health Grants R01 HL80186 (WJD), R21 HL109693 (WJD), PO1 HL 62426 (RJS), and by the M. J. Murdock Charitable Trust (WJD), and by American Heart Association grants 17GRNT33460153 (WJD).

Abbreviations

cTnC	cardiac troponin C
cTnI	cardiac troponin I
cTnT	cardiac troponin T
cTnI-MD	mobile domain of cardiac troponin I
cTnI(WT)	wild-type cTnI

SL	sarcomere length
LDA	length dependent activation
N-cTnC	N-domain of cTnC
FRET	Förster resonance energy transfer
Vanadate	Vi
BES	N,N-Bis(2-hydroxyethyl)-2-aminoethanesulfonic acid
EGTA	ethylene glycol-bis(β-aminoethyl ether)-N,N,N′,N′-tetraacetic acid
DTT	Dithiothreitol
BDM	2,3-Butanedione monoxime
HWHM	half-width at half-maximum

References

1. Lakatta EG. Starling's law of the heart is explained by an intimate interaction of muscle length and myofilament calcium activation. J Am Coll Cardiol. 1987; 10(5):1157–1164. [PubMed: 3312367]
2. Allen DG, Kentish JC. The cellular basis of the length-tension relation in cardiac muscle. J Mol Cell Cardiol. 1985; 17(9):821–40. [PubMed: 3900426]
3. Fuchs F, Smith SH. Calcium, cross-bridges, and the Frank-Starling relationship. News Physiol Sci. 2001; 16:5–10. [PubMed: 11390938]
4. Kentish JC, et al. Comparison between the sarcomere length-force relations of intact and skinned trabeculae from rat right ventricle. Influence of calcium concentrations on these relations. Circulation Research. 1986; 58(6):755–68. [PubMed: 3719928]
5. Hibberd MG, Jewell BR. Calcium- and length-dependent force production in rat ventricular muscle. The Journal of Physiology. 1982; 329(1):527–540. [PubMed: 7143258]
6. Allen DG, Kurihara S. The effects of muscle length on intracellular calcium transients in mammalian cardiac muscle. The Journal of Physiology. 1982; 327:79–94. [PubMed: 7120151]
7. Fabiato A, Fabiato F. Dependence of the contractile activation of skinned cardiac cells on the sarcomere length. Nature. 1975; 256(5512):54–56. [PubMed: 1134580]
8. de Tombe PP, et al. Myofilament length dependent activation. J Mol Cell Cardiol. 2010; 48(5):851–858. [PubMed: 20053351]
9. Huxley HE. Structural changes in the actin-and myosin-containing filaments during contraction. Cold Spring Harbor Symp Qant Biol. 1972; 37:361–376.
10. Li KL, et al. In situ time-resolved FRET reveals effects of sarcomere length on cardiac thin-filament activation. Biophys J. 2014; 107(3):682–93. [PubMed: 25099807]
11. de Tombe PP. Cardiac myofilaments: mechanics and regulation. J Biomech. 2003; 36(5):721–30. [PubMed: 12695002]
12. Kobayashi T, Jin L, de Tombe PP. Cardiac thin filament regulation. Pflugers Arch. 2008; doi: 10.1007/s00424-008-0511-8
13. McDonald KS, Moss RL. Osmotic compression of single cardiac myocytes eliminates the reduction in Ca2+ sensitivity of tension at short sarcomere length. Circ Res. 1995; 77(1):199–205. [PubMed: 7788878]
14. Fuchs F, Wang YP. Sarcomere Length Versus Interfilament Spacing as Determinants of Cardiac Myofilament Ca2+Sensitivity and Ca2+Binding. J Mol Cell Cardiol. 1996; 28(7):1375–1383. [PubMed: 8841926]

15. Irving TC, et al. Myofilament lattice spacing as a function of sarcomere length in isolated rat myocardium. Am J Physiol Heart Circ Physiol. 2000; 279(5):H2568–73. [PubMed: 11045995]
16. Irving T, et al. Thick-Filament Strain and Interfilament Spacing in Passive Muscle: Effect of Titin-Based Passive Tension. Biophysical Journal. 2011; 100(6):1499–1508. [PubMed: 21402032]
17. Fukuda N, et al. Titin-based modulation of active tension and interfilament lattice spacing in skinned rat cardiac muscle. Pflugers Arch. 2005; 449(5):449–57. [PubMed: 15688246]
18. Cazorla O, et al. Titin-based modulation of calcium sensitivity of active tension in mouse skinned cardiac myocytes. Circ Res. 2001; 88(10):1028–35. [PubMed: 11375272]
19. Methawasin M, et al. Experimentally increasing titin compliance in a novel mouse model attenuates the Frank-Starling mechanism but has a beneficial effect on diastole. Circulation. 2014; 129(19):1924–36. [PubMed: 24599837]
20. Fukuda N, et al. Length dependence of tension generation in rat skinned cardiac muscle: role of titin in the Frank-Starling mechanism of the heart. Circulation. 2001; 104(14):1639–45. [PubMed: 11581142]
21. Fukuda N, et al. Sarcomere length-dependent Ca2+ activation in skinned rabbit psoas muscle fibers: coordinated regulation of thin filament cooperative activation and passive force. J Physiol Sci. 2011; 61(6):515–23. [PubMed: 21901640]
22. Farman GP, et al. Myosin head orientation: a structural determinant for the Frank-Starling relationship. Am J Physiol - Heart C. 2011; 300(6):H2155–H2160.
23. Farman GP, et al. Impact of osmotic compression on sarcomere structure and myofilament calcium sensitivity of isolated rat myocardium. Am J Physiol - Heart C. 2006; 291(4):H1847–H1855.
24. Fusi L, et al. Thick filament mechano-sensing is a calcium-independent regulatory mechanism in skeletal muscle. Nature Communications. 2016; 7:13281.
25. Zhang X, et al. Distinct contributions of the thin and thick filaments to length-dependent activation in heart muscle. eLife. 2017; 6:e24081. [PubMed: 28229860]
26. Reconditi M, et al. Sarcomere-length dependence of myosin filament structure in skeletal muscle fibres of the frog. J Physiol. 2014; 592(5):1119–37. [PubMed: 24344169]
27. Adhikari BB, et al. Cardiac Length Dependence of Force and Force Redevelopment Kinetics with Altered Cross-Bridge Cycling. Biophysical Journal. 2004; 87(3):1784–1794. [PubMed: 15345557]
28. Regnier M, et al. Cross-Bridge versus Thin Filament Contributions to the Level and Rate of Force Development in Cardiac Muscle. Biophys J. 2004; 87:1815–1824. [PubMed: 15345560]
29. Fitzsimons DP, Moss RL. Strong binding of myosin modulates length-dependent Ca^{2+} activation of rat ventricular myocytes. Circ Res. 1998; 83(6):602–607. [PubMed: 9742055]
30. Moreno-Gonzalez A, Fredlund J, Regnier M. Cardiac troponin C (TnC) and a site I skeletal TnC mutant alter Ca2+ versus crossbridge contribution to force in rabbit skeletal fibres. J Physiol. 2005; 562(Pt 3):873–84. [PubMed: 15611027]
31. Fukuda N, et al. Effects of MgADP on length dependence of tension generation in skinned rat cardiac muscle. Circ Res. 2000; 86(1):e1–e6. [PubMed: 10625312]
32. Liang B, et al. Ca2+ regulation of rabbit skeletal muscle thin filament sliding: role of cross-bridge number. Biophys J. 2003; 85(3):1775–86. [PubMed: 12944292]
33. Bremel RD, Weber A. Cooperation within actin filament in vertebrate skeletal muscle. Nature New Biol. 1972; 238(82):97–101. [PubMed: 4261616]
34. Pan BS, Solaro RJ. Calcium-binding properties of troponin C in detergent-skinned heart muscle fibers. J Biol Chem. 1987; 262(16):7839–7849. [PubMed: 3584144]
35. Allen DG, Kentish JC. Calcium concentration in the myoplasm of skinned ferret ventricular muscle following changes in muscle length. The Journal of Physiology. 1988; 407:489–503. [PubMed: 3151492]
36. Moss RL, Razumova M, Fitzsimons DP. Myosin crossbridge activation of cardiac thin filaments: implications for myocardial function in health and disease. Circ Res. 2004; 94(10):1290–300. [PubMed: 15166116]
37. Lehrer S. The 3-state model of muscle regulation revisited: is a fourth state involved? J Muscle Res Cell M. 2011; 32(3):203–208.

38. Hinken AC, Solaro RJ. A dominant role of cardiac molecular motors in the intrinsic regulation of ventricular ejection and relaxation. Physiology (Bethesda). 2007; 22:73–80. [PubMed: 17420299]
39. Rieck DC, et al. Structural basis for the in situ Ca(2+) sensitization of cardiac troponin C by positive feedback from force-generating myosin cross-bridges. Arch Biochem Biophys. 2013; 537(2):198–209. [PubMed: 23896515]
40. Tobacman LS. Thin Filament-Mediated Regulation of Cardiac Contraction. Annual Review of Physiology. 1996; 58(1):447–481.
41. Gordon AM, Homsher E, Regnier M. Regulation of contraction in striated muscle. Physiol Rev. 2000; 80(2):853–924. [PubMed: 10747208]
42. Wei B, Jin JP. Troponin T isoforms and posttranscriptional modifications: Evolution, regulation and function. Arch Biochem Biophys. 2011; 505(2):144–154. [PubMed: 20965144]
43. Behrmann E, et al. Structure of the rigor actin-tropomyosin-myosin complex. Cell. 2012; 150(2): 327–38. [PubMed: 22817895]
44. Li MX, Spyracopoulos L, Sykes BD. Binding of cardiac troponin-I147-163 induces a structural opening in human cardiac troponin-C. Biochemistry. 1999; 38(26):8289–98. [PubMed: 10387074]
45. Dong WJ, et al. Conformation of the regulatory domain of cardiac muscle troponin C in its complex with cardiac troponin I. J Biol Chem. 1999; 274(44):31382–90. [PubMed: 10531339]
46. Dong WJ, et al. Ca^{2+} induces an extended conformation of the inhibitory region of troponin I in cardiac muscle troponin. J Mol Biol. 2001; 314(1):51–61. [PubMed: 11724531]
47. Dong WJ, et al. Ca2+-induced conformational transition in the inhibitory and regulatory regions of cardiac troponin I. J Biol Chem. 2003; 278(10):8686–92. [PubMed: 12511564]
48. Kobayashi T, et al. Inhibitory region of troponin I: Ca(2+)-dependent structural and environmental changes in the troponin-tropomyosin complex and in reconstituted thin filaments. Biochemistry. 2000; 39(1):86–91. [PubMed: 10625482]
49. Robinson JM, et al. Switching of troponin I: Ca(2+) and myosin-induced activation of heart muscle. J Mol Biol. 2004; 340(2):295–305. [PubMed: 15201053]
50. Xing J, et al. Structural studies of interactions between cardiac troponin I and actin in regulated thin filament using Forster resonance energy transfer. Biochemistry. 2008; 47(50):13383–93. [PubMed: 19053249]
51. Xing J, et al. Forster resonance energy transfer structural kinetic studies of cardiac thin filament deactivation. J Biol Chem. 2009; 284(24):16432–41. [PubMed: 19369252]
52. Zhou Z, et al. Structural dynamics of C-domain of cardiac troponin I protein in reconstituted thin filament. J Biol Chem. 2012; 287(10):7661–74. [PubMed: 22207765]
53. Li KL, et al. Sarcomere length dependent effects on the interaction between cTnC and cTnI in skinned papillary muscle strips. Arch Biochem Biophys. 2016; 601:69–79. [PubMed: 26944554]
54. Gomes AV, Potter JD, Szczesna-Cordary D. The role of troponins in muscle contraction. IUBMB Life. 2002; 54(6):323–33. [PubMed: 12665242]
55. de Tombe PP, et al. Myofilament length dependent activation. J Mol Cell Cardiol. 2010; 48(5):851–8. [PubMed: 20053351]
56. Bohlooli Ghashghaee N, Tanner BCW, Dong W-J. Functional significance of C-terminal mobile domain of cardiac troponin I. Archives of Biochemistry and Biophysics. 2017; 634(Supplement C):38–46. [PubMed: 28958680]
57. Arteaga GM, et al. Attenuation of length dependence of calcium activation in myofilaments of transgenic mouse hearts expressing slow skeletal troponin I. J Physiol. 2000; 526:541–549. [PubMed: 10922006]
58. Tripet B, Van Eyk JE, Hodges RS. Mapping of a second actin-tropomyosin and a second troponin C binding site within the C terminus of troponin I, and their importance in the Ca2+-dependent regulation of muscle contraction. J Mol Biol. 1997; 271(5):728–750. [PubMed: 9299323]
59. Murakami K, et al. Structural basis for Ca2+-regulated muscle relaxation at interaction sites of troponin with actin and tropomyosin. J Mol Biol. 2005; 352(1):178–201. [PubMed: 16061251]
60. Galińska A, et al. The C-terminus of cardiac troponin I stabilizes the Ca(2+)-activated state of tropomyosin on actin filaments. Circulation research. 2010; 106(4):705–711. [PubMed: 20035081]

61. Hoffman RMB, Blumenschein TMA, Sykes BD. An Interplay between Protein Disorder and Structure Confers the Ca2+ Regulation of Striated Muscle. Journal of Molecular Biology. 2006; 361(4):625–633. [PubMed: 16876196]
62. Blumenschein TM, et al. Calcium-dependent changes in the flexibility of the regulatory domain of troponin C in the troponin complex. J Biol Chem. 2005; 280(23):21924–32. [PubMed: 15826946]
63. Blumenschein TM, et al. Dynamics of the C-terminal region of TnI in the troponin complex in solution. Biophys J. 2006; 90(7):2436–44. [PubMed: 16415057]
64. Kowlessur D, Tobacman LS. Troponin regulatory function and dynamics revealed by H/D exchange-mass spectrometry. J Biol Chem. 2010; 285(4):2686–94. [PubMed: 19920153]
65. Kowlessur D, Tobacman LS. Significance of troponin dynamics for Ca^{2+}-mediated regulation of contraction and inherited cardiomyopathy. J Biol Chem. 2012; 287(50):42299–311. [PubMed: 23066014]
66. Shoemaker BA, Portman JJ, Wolynes PG. Speeding molecular recognition by using the folding funnel: the fly-casting mechanism. Proc Natl Acad Sci U S A. 2000; 97(16):8868–73. [PubMed: 10908673]
67. Fabiato A, Fabiato F. Calculator programs for computing the composition of the solutions containing multiple metals and ligands used for experiments in skinned muscle cells. J Physiol (Paris). 1979; 75(5):463–505. [PubMed: 533865]
68. Chandra M, et al. Interaction between myosin heavy chain and troponin isoforms modulate cardiac myofiber contractile dynamics. Am J Physiol Regul Integr Comp Physiol. 2007; 293(4):R1595–607. [PubMed: 17626127]
69. Terui T, et al. Regulatory mechanism of length-dependent activation in skinned porcine ventricular muscle: role of thin filament cooperative activation in the Frank-Starling relation. J Gen Physiol. 2010; 136(4):469–82. [PubMed: 20876361]
70. Campbell KS. Impact of myocyte strain on cardiac myofilament activation. Pflugers Arch. 2011; 462(1):3–14. [PubMed: 21409385]
71. Mocz G. Vanadate-mediated photocleavage of rabbit skeletal myosin. Eur J Biochem. 1989; 179(2):373–8. [PubMed: 2537208]
72. Fukuda N, et al. Titin and troponin: central players in the frank-starling mechanism of the heart. Curr Cardiol Rev. 2009; 5(2):119–24. [PubMed: 20436852]
73. Strauss JD, et al. Troponin replacement in permeabilized cardiac muscle reversible extraction of troponin I by incubation with vanadate. FEBS Letters. 1992; 310(3):229–234. [PubMed: 1397278]
74. Liao R, Wang CK, Cheung HC. Time-resolved tryptophan emission study of cardiac troponin I. Biophys J. 1992; 63(4):986–95. [PubMed: 1420937]
75. Spyracopoulos L, et al. Calcium-induced structural transition in the regulatory domain of human cardiac troponin C. Biochemistry. 1997; 36(40):12138–46. [PubMed: 9315850]

Highlights

- cTnI(1-167) perturbs the thin filament-based regulatory mechanisms of length dependent activation.
- cTnI(1-167) uncouples the thin and thick filament-based regulations of length dependent activation.
- cTnI(1-167) promotes the opening of the N-cTnC hydrophobic cleft at short SL.
- cTnI(1-167) diminishes the sarcomere length-induced opening of N-cTnC.
- The cTnI(1-167) effects on thin filament activation are more pronounced at short SL.

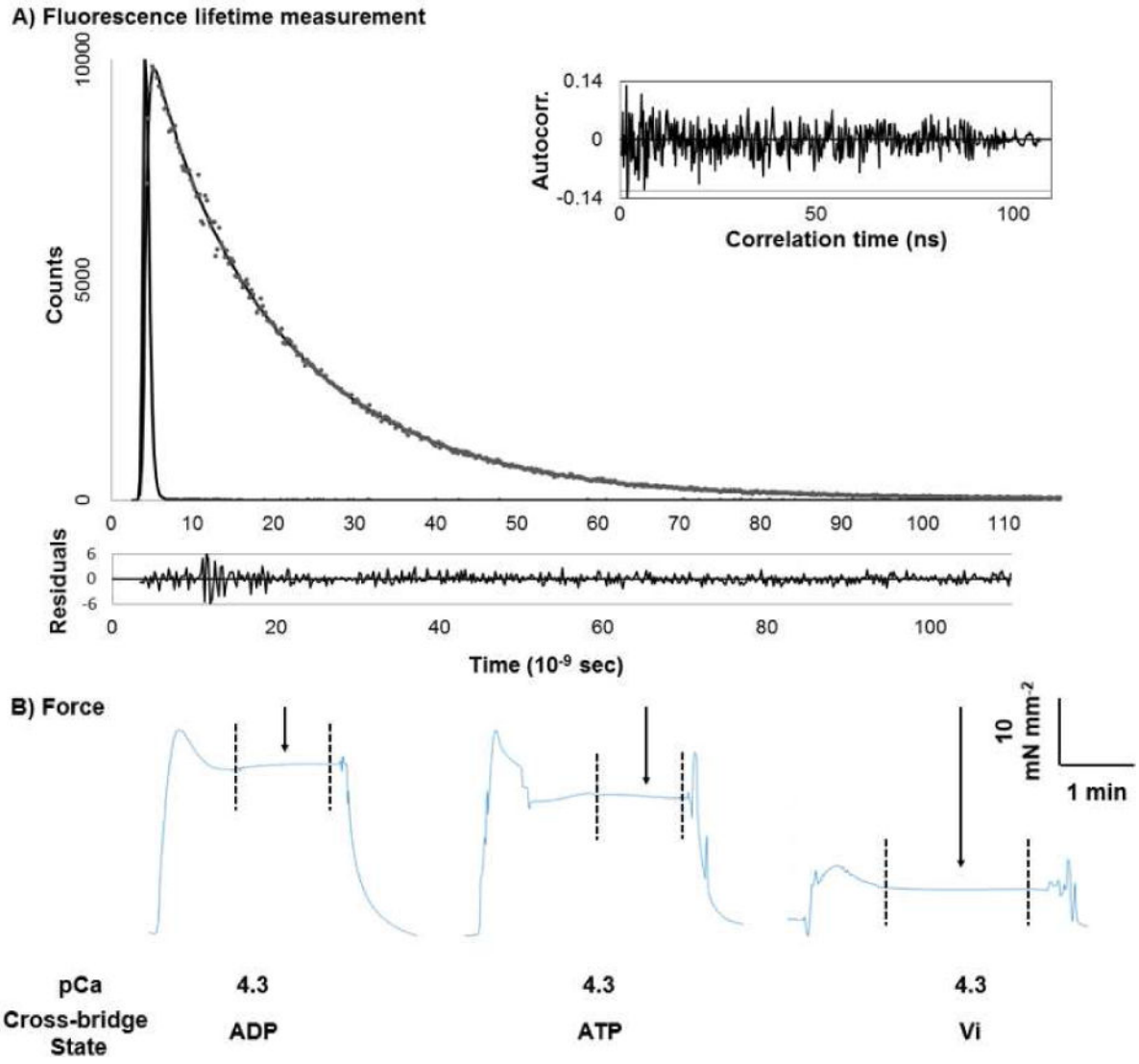

Figure 1.

Protocol scheme for simultaneous fluorescence lifetime decay and isometric force performed in detergent skinned papillary muscle fibers. (A) represents the trace of the total intensity fluorescence decay for fibers containing FRET donor (AEDANS) in presence of non-fluorescent acceptor (DDPM) (grey dots), which was measured at 1.8 μm SL at pCa 4.3. The decay data was fitted with Eq. (2) (black line). The autocorrect (inset) and residual (lower panel) were used to judge the goodness of fit. (B) Fluorescence intensity decays were measured when force had reached steady state as indicated by the arrows and dash lines. The example force traces were measured at pCa 4.3 at indicated cross-bridge state. The magnitudes of force and time are indicated by the horizontal and vertical bars.

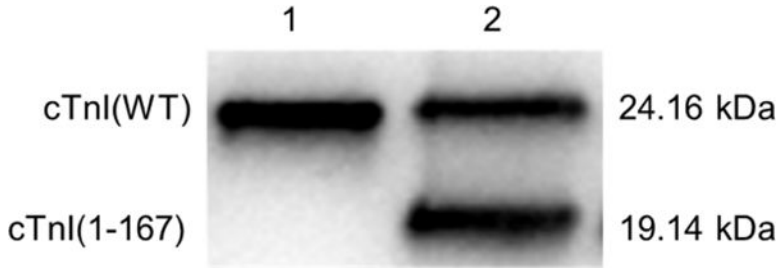

Figure 2.

Western blot analysis of reconstituted cardiac muscle preparations. Anti-cTnI antibody was used to assess the level of the incorporation of cTnI(1-167) into the reconstituted cardiac muscle preparations. Starting from the left, lanes 1and 2 shows cTnI(WT) and cTnI(1-167) reconstituted cardiac muscle fibers, respectively. Image J software was used for densitometric analysis of band intensities and the relative amount of incorporated cTnI(1-167) was 60% ± 4 (n=3).

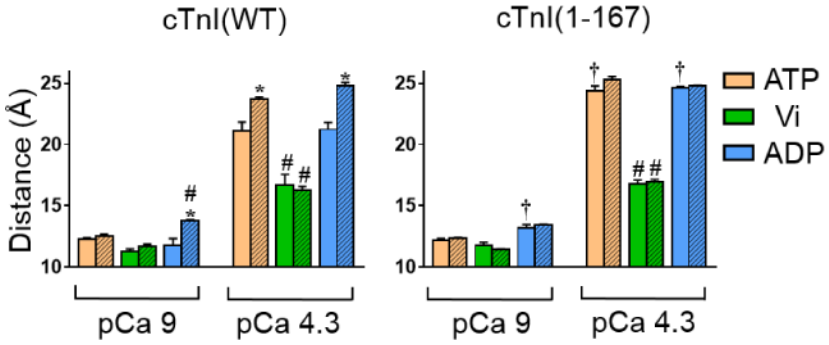

Figure 3.

Comparison of N-cTnC Cys-13–Cys-51 distance distributions as a function of cTnC site-II Ca^{2+} occupancy (pCa 9 and 4.3) and cross-bridge binding state (ATP, Vi, and ADP) when observed at 1.8μm (solid bars) and 2.2 μm (hatched bars) SLs in cTnC(T13C/N51C)$_{AEDANS\text{-}DDPM}$-reconstituted myocardial fibers containing recombinant cTnI(WT)-left panel or cTnI(1-167)-right panel.

*: Effect of SL for wild-type or truncated cTnI; $P<0.05$

†: Truncation effect compared to cTnI(WT) at same SL, cross-bridge state, and pCa; $P<0.05$

#: Effect of cross-bridge state compared to ATP state at same SL and pCa for wild-type or truncated cTnI; $P<0.05$

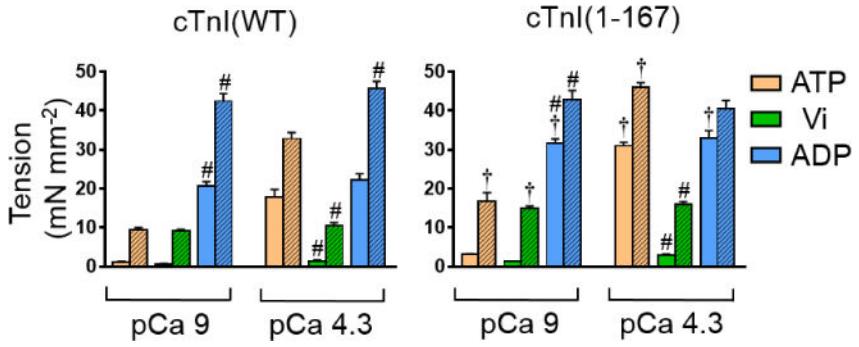

Figure 4.

Comparison of steady state maximal tension as a function of cTnC site-II Ca^{2+} occupancy (pCa 9 and 4.3) and cross-bridge binding state (ATP, Vi, and ADP) when observed at 1.8μm (solid bars) and 2.2μm (hatched bars) SLs in cTnC(T13C/N51C)$_{AEDANS\text{-}DDPM}$-reconstituted myocardial fibers containing recombinant cTnI(WT)-left panel or cTnI(1-167)-right panel. Increase in SL resulted in a greater maximal tension at all cross-bridge states and pCa conditions for both wild-type and truncated cTnI fibers.

†: Truncation effect compared to cTnI(WT) at same SL, cross-bridge state, and pCa; $P<0.05$

#: Effect of cross-bridge state compared to ATP state at same SL and pCa for wild-type or truncated cTnI; $P<0.05$

Table 1

Cys-13–Cys-51 distance distributions and force values observed in cTnC(N13C/T51C)$_{AEDANS-DDPM}$-reconstituted fibers containing cTnI(1-167) or cTnI(WT) under different biochemical conditions. Absolute parameter values are given as mean ± SEM.

		r^a (Å)		*HWHM*^{b} (Å)		Force (mN mm^{-2})	
Cross-bridge state	**pCa**	**1.8 μm SL**	**2.2 μm SL**	**1.8 μm SL**	**2.2 μm SL**	**1.8 μm SL**	**2.2 μm SL**
cTnI(1-167)	9	12.21 ± 0.11	12.36 ± 0.06	6.36 ± 0.82	6.47 ± 0.57†	3.10 ± 0.11	16.80 ± 2.16*†
ATP(5 mM)	4.3	24.37 ± 0.42†	25.31 ± 0.26	5.08 ± 0.83	5.85 ± 0.46†	30.97± 0.92†	45.88 ± 1.35*†
cTnI(WT)	9	12.30 ± 0.09	12.50 ± 0.21	6.48 ± 0.08	8.29 ± 0.15*	1.04 ± 0.15	9.54 ± 0.48*
ATP(5 mM)	4.3	21.12 ± 0.74	23.72 ± 0.20*	7.20 ± 0.35	9.86 ± 0.68*	17.78 ± 1.98	32.83 ± 1.59*
cTnI(1-167)	9	11.79 ± 0.23	11.40 ± 0.08	6.70 ± 0.23	6.58 ± 0.15	1.23 ± 0.13	14.81 ± 0.75*†
Vi^c(1 mM)	4.3	16.76 ± 0.36$^{\#}$	16.98 ± 0.18$^{\#}$	6.45 ± 0.35	6.98 ± 0.28	2.93 ± 0.17$^{\#}$	15.89 ± 0.80$^{*\#}$
cTnI(WT)	9	11.27 ± 0.21	11.69 ± 0.19	6.01 ± 0.18	6.03 ± 0.08$^{\#}$	0.65 ± 0.07	9.24 ± 0.29*
Vi^c(1 mM)	4.3	16.68 ± 0.90$^{\#}$	16.30 ± 0.29$^{\#}$	6.50 ± 0.50	6.61 ± 0.44$^{\#}$	1.39 ± 0.12$^{\#}$	10.53 ± 0.74$^{*\#}$
cTnI(1-167)	9	13.21 ± 0.26†	13.42 ± 0.10	6.45 ± 0.21	6.22 ± 0.28	31.65 ± 1.11$^{\dagger\#}$	42.90 ± 2.30$^{*\#}$
ADP^d(5 mM)	4.3	24.64 ± 0.13†	24.79 ± 0.06	5.07 ± 0.48	5.29 ± 0.38	32.95 ± 1.93†	40.59 ± 2.07*
cTnI(WT)	9	11.78 ± 0.55	13.81 ± 0.08$^{*\#}$	6.59 ± 0.14	6.47 ± 0.22$^{\#}$	20.62 ± 1.19$^{\#}$	42.46 ± 1.96$^{*\#}$
ADP^d(5 mM)	4.3	21.26 ± 0.56	24.82 ± 0.27*	6.82 ± 0.59	5.89 ± 0.32$^{\#}$	22.22 ± 1.59	45.67 ± 1.86$^{*\#}$

[a] r is the mean distance associated with the distribution.

[b] *HWHM* denotes the half width at half maximum.

[c] Vi solutions also contained 5 mM ATP.

[d] ATP was absent in ADP solutions.

*: Effect of SL for each truncation or wild-type; $P<0.05$

†: Truncation effect compared to cTnI(WT) at same SL, cross-bridge state, and pCa; $P<0.05$

$^{\#}$: Effect of cross-bridge state compared to ATP state at same truncation, SL, and pCa; $P<0.05$